PCCP

Accepted Manuscript

ROYAL SOCIETY OF CHEMISTRY

www.rsc.org/pccp

PCCP

RSCPublishing

ARTICLE

The Positions of Inner Hydroxide Groups and Aluminium Ions in Exfoliated Kaolinite as Indicators for External Chemical Environment

Cite this: DOI: 10.1039/xoxxoooooox

Received 11th August 2014,
Accepted 11th August 2014

DOI: 10.1039/xoxxoooooox

www.rsc.org/

Attila Táborosi,[a] Róbert Kurdi,[a] and Róbert K. Szilágyi[b,c],

Kaolinite as a remarkable industrial raw material has notable structural features despite its simple chemical composition ($Al_2O_3 \cdot 2SiO_2 \cdot 2H_2O$). We report here a systematic development of a coordination chemical model for the [6Al-6(OH)] honeycomb-like unit of the kaolinite's octahedral sheet, which was proposed to be the adsorption site for small molecules from earlier studies. The coordination environment of the Al^{3+} ions was completed with outer sphere groups from both octahedral and tetrahedral sheets. Dangling bonds were terminated by additional Al^{3+} and Si^{4+} ions with hydroxide and oxide groups from the second coordination sphere *versus* simple protonation. A cage of Na^{+} and Mg^{2+} ions rendered the computational model to be charge neutral. In this exfoliated kaolinite model, the inner hydroxide groups and the adjacent Al^{3+} ions have compositionally the most complete environments with respect to the crystal structure. Thus, their atomic positions were used as benchmark for the level of theory dependence of the optimized structures. We evaluated the performance of a representative set of density functionals, basis sets, point-charges, identified pitfalls and caveats. Importantly, the structural changes during optimizations of periodic and cluster models suggest pliability for the exfoliated kaolinite layers, which is influenced by the external chemical environment.

Introduction

Clay minerals are emerging hard materials with industrial relevance. Their applications greatly depend on their surface properties.[1] Separation of adjacent clay layers (delamination) and elimination of the crystallographic order (exfoliation) alter their morphology and thus the industrial value of clay-based nanoparticles. The exfoliated clay layers are of great interest due to their high surface area and functionalizability. The current approach for designing and optimizing delamination and exfoliation processes are dominantly empirical trial-and-error. The use of computer-aided rationalized design allows for direct and economical preparation of nanoscale clay specimens and hybrid materials containing organic and/or inorganic reagents with tailored physical and chemical properties. An essential step to this approach is to develop and validate computational models for gaining understanding of structure and property relationships in clays at the molecular level.

A common computational approach is the employment of periodic boundary conditions given the periodic nature of clay minerals.[2-13] This approach is preferred when the emphasis is on periodicity of the structure and properties. However, for nanomaterials where the periodicity can be reduced or even completely eliminated as in tubes or chips of exfoliated kaolinite sheets, at the edges of kaolinite layers, and in the presence of clustered transition metal contaminations, an alternative approach can be used that employs molecular scale, cluster models.[14-22] The benefit of using molecular models is the possibility of focusing in on localized defect sites, presence of substitutions, lack of atoms/ions, and adsorption/reactivity of exogenous molecules. Furthermore, a broader range of computational methods is available for electronic structure analysis and potential energy surface studies of chemical reactivity for cluster models *versus* periodic boundary models.

The given study focuses on kaolinite as the simplest example for phylloaluminosilicate. The exfoliated kaolinite (Scheme 1) is composed of a single pair of covalently linked octahedral (O) and tetrahedral (T) sheets. The stacking sequence [···OT···OT···] classifies kaolinite as a member of the 1:1 clay mineral group. The inner sphere coordination environment of a hexacoordinate Al^{3+} ion contains three surface

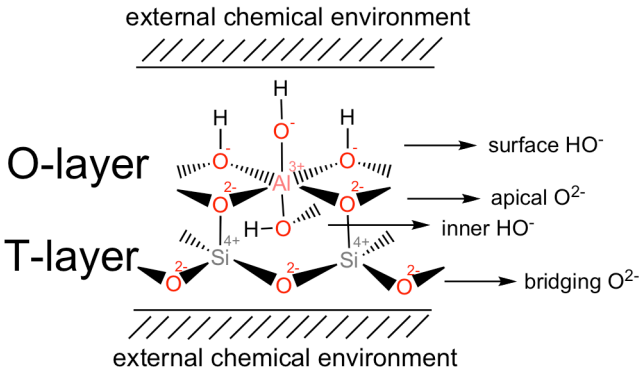

Scheme 1 Representation of coordination environments in exfoliated kaolinite

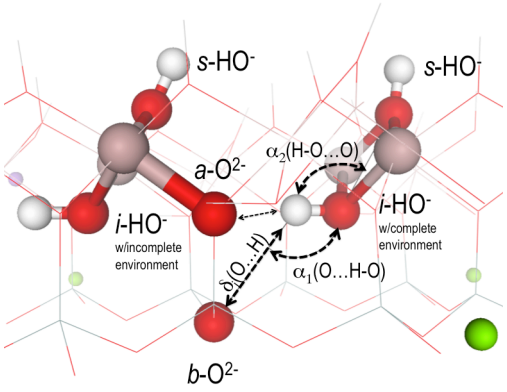

Fig. 1 A set of representative internal coordinates (b-$O^{2-}\cdots$H-O(i-HO^-) distance δ and angle α_1, H-O(i-HO^-)$\cdots$O(s-HO^-) angle α_2) describing the position of i-HO^- (green and purple spheres are Mg^{2+} and Na^+ neutralizing counter ions)

hydroxides (s-HO^-), an inner hydroxide (i-HO^-), and two apical oxide (a-O^{2-}) groups. The Si^{4+} ions of the T-sheet are linked *via* the bridging oxides (b-O^{2-}). The s-HO^- groups connect two separate OT layers *via* hydrogen bonds (H-bonds) in b-$O^{2-}\cdots$H-O(s-HO^-). The apical oxides (a-O^{2-}) connect the O- and T-sheets within an OT layer, while the i-HO^- group bridges two adjacent Al^{3+} within the O-sheet without a direct covalent connection to the T-sheet.

Hereby, we report our quantum chemical modelling to establish a realistic cluster model for studying adsorption, intercalation, and organocomplex formation in phyllosilicates.[23, 24] The modelling strategy originates from practices accepted for metalloenzymes, where the reactive inorganic sites of interest (often sizeable metalloclusters[25, 26]) are embedded into a matrix of soft materials (protein environment).[27] In clay minerals, the sites of interests are embedded into a hard material environment as defined by the crystalline phase. There are fundamental differences between the low dielectric, but highly covalent soft-material and the ionic, but less covalent hard material; however, following the general coordination chemistry principles with respect to inner and outer sphere environments these differences can be gauged and adequately treated. A key step is the careful examination of the computational level of theory and point-charge dependence of the computational results. As an independent approach, we carried out comparative periodic model calculations in support of the applicability of the cluster model for exfoliated kaolinite.

We emphasize the importance of considering coordination chemistry principles when establishing molecular cluster models including the appropriate termination of the model with counter ions for obtaining charge neutrality *versus* truncating models to mitigate computational cost. The coordination chemistry approach ensures that structural changes observed by modelling correspond to real structural changes *versus* errors due to truncated model or limitations of a level of theory and basis set. The employed large-scale computational model with 136 atoms with 20 counter ions enabled a realistic structural representation of the complete chemical environment for an $[Al^{3+}\cdots s\text{-}HO^-]_6$ honeycomb-like unit (Fig. 2A) with the centrally located i-HO^- group (Fig. 1) in an exfoliated kaolinite layer. The i-HO^- position in the crystal structure can be characterized by four non-ideal, bent H-bonds (thin arrow at the centre of Fig. 1) involving two a-O^{2-} groups between the T- and O-sheets at 2.63 Å and 2.83 Å H$\cdots$O distances (δ) and ca. 140º and 80º O-

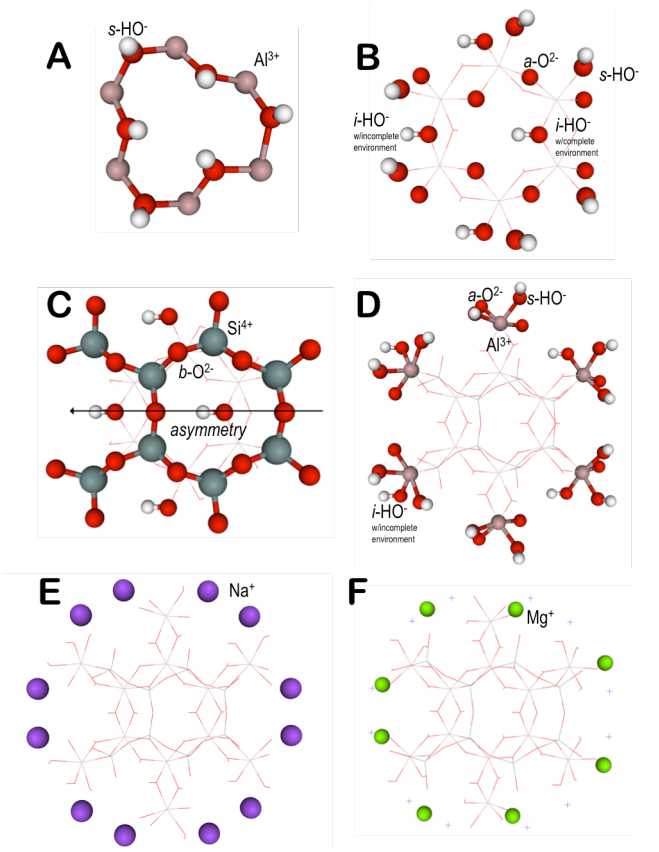

Fig. 2 Definition of various chemical environments for a large-scale molecular cluster model for exfoliated kaolinite (A: honeycomb of the O-sheet; B: hydroxide and oxide groups completing the inner coordination sphere; C: honeycomb for the T-sheet with extra Si^{4+} tetrahedrons due to T/O-sheet misfit; D: $[Al^{3+}(HO^-)_{2\text{ or }3}(O^{2-})_{3\text{ or }2}]$ fragments completing the outer coordination sphere; E and F: Na^+ and Mg^{2+} ions at the positions of Al^{3+} and Si^{4+} ions from the third coordination sphere to the central O-sheet honeycomb, respectively)

H$\cdots$O angles (α_1), respectively. Given the long distances and the non-ideal donor-H…acceptor bond angles, these weak H-bonds have dominantly a charge/dipole nature with negligible covalent character. Another notable geometric feature of the i-HO^- group is the close to parallel orientation of the H-O(i-HO^-) bond relative to plane of the Al^{3+} ions or the (001) plane of the kaolinite lattice. This can be characterized by the tilt of the $[Al^{3+}\cdots i\text{-}HO^-/s\text{-}HO^-]_2$ rhomb. The O(s-HO^-)$\cdots$O-H(i-HO^-) angle (α_2) has a value of 120º in the crystal structure of kaolinite.

Methodology

Computational Details

The reference structure for the computational model was based on the combined experimental (X-ray and neutron diffraction) and computational (periodic model with PW91 density functional) study,[28] where all atomic positions, including the H atoms were refined. The structural data were obtained from the FIZ Karlsruhe Inorganic Structural Database [29, 30] (structure reference number 078401).

Development of the Cluster Model

We chose the $[Al^{3+}\cdots s\text{-}HO^-]_6$ honeycomb-like unit (Fig. 2A) as a site of interest for the coordination chemical model of the

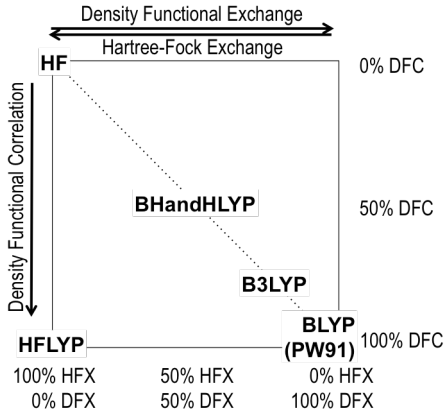

Scheme 2 Connection among the level of theories used in the given study

Table 1 Summary of point-charges considered for construction of an about 25 Å × 25 Å field of point-charges around the cluster model of the exfoliated OT-sheet of kaolinite (UFF QEq: Universal Force Field with charge equilibration method;[57-58] PM6: semi-empirical Hamiltonian and parameter set;[59-60] MPA: Mulliken Population Analysis,[61] NPA: Natural Population Analysis)[61-64]

	UFF	PM6	HF-TZ		PW91-TZ	
ions	QEq	MPA	MPA	NPA	MPA	NPA
Al^{3+}	1.11	1.37	1.10	2.18	0.58	2.06
Si^{4+}	1.31	0.56	1.05	2.63	0.52	2.43
O^{2-} (surface)	-0.71	-0.74	-0.66	-1.21	-0.46	-1.19
H^{+} (surface)	0.21	0.29	0.31	0.48	0.28	0.49
O^{2-} (inner)	-0.73	-0.64	-0.68	-1.22	-0.48	-1.18
H^{+} (inner)	0.25	0.33	0.34	0.50	0.28	0.51
O^{2-} (apical)	-0.55	-0.63	-0.62	-1.42	-0.27	-1.35
O^{2-} (bridging)	-0.60	-0.35	-0.46	-1.32	-0.29	-1.22

exfoliated kaolinite as proposed by recent cluster-based modelling efforts.[17, 18, 20-22, 31, 32] for the preferred site of adsorption. The central building block of the cluster model will represent an "active site" with respect to adsorption that is to be embedded in a hard material environment following coordination chemistry principles. Therefore, in addition to the two *s*-HO^- groups from the central unit (Fig. 2A), each Al^{3+} ion's coordination environment was completed with two *a*-O^{2-} groups that bridges adjacent Al^{3+} ions and connects the O-sheet to the Si^{4+} ions of the T-sheet and two additional buried *i*-HO^- ions (Fig. 2B). The $[(Al^{3+})_6(s\text{-}HO^-)_{12}(i\text{-}HO^-)_6(a\text{-}O^{2-})_6]^{12-}$ model with various termination strategies at the periphery and charge neutralization is a common model in literature.[17, 21, 31] However, this model is not yet acceptable if coordination chemical principles are considered. The dangling hydroxide and oxide groups require extension of this model with outer coordination sphere in order to create a realistic chemical environment for the central $[Al^{3+}\cdots s\text{-}HO^-]_6$ honeycomb-like unit. Therefore, adjacent Si^{4+} ions of the T-sheet were included with *b*-O^{2-} groups to complete their tetrahedral coordination environment. This extension completes a $[Si^{4+}\cdots b\text{-}O^{2-}]_6$ honeycomb that has a misfit relative to the $[Al^{3+}\cdots s\text{-}HO^-]_6$ honeycomb. The slip between the two honeycombs requires the inclusion of two additional Si^{4+} ions with their *b*-O^{2-} groups. This creates an asymmetry in the model along the direction of the H-O bond of *i*-HO^- groups (Fig. 2C). The proximal position of hydroxide groups from the outer coordination sphere is expected to have a measurable electronic affect on the structural features of the central unit; therefore, we extended the first outer sphere with additional four $[Al^{3+}(HO^-)_2(O^{2-})_2]$ and two $[Al^{3+}(HO^-)_3(O^{2-})]$ ionic fragments (Fig. 2D) parallel and perpendicular to the asymmetry of the cluster model, respectively. Furthermore, we employed 12 Na^+ and 8 Mg^{2+} counter ions to neutralize the model's negative charge. These ions were chosen as a compromise of ionic size and orbital radial function in comparison to using protons, smaller ions with more covalent character and smaller size (Li^+/Be^{2+}), or larger ions with no covalent bonding (Cs^+, Ba^{2+}). The Na^+ ions were placed at the positions of second outer sphere Al^{3+} ions that are about 7 Å away from the central *i*-HO^- group (Fig. 2E). The positions of the Mg^{2+} ions match those of the second outer sphere Si^{4+} ions (Fig. 2F). While the 7 Å can be still considered a distance for considerable Coulomb interactions; however, the outer coordination spheres screen the neutralizing counter ions. The effect of neutralizing cage of cations was evaluated by embedding the cluster model into a field of 460 point-charges calculated at various levels of theory (Table 1). The positions of the point-charges were obtained from the 5×5 slab of the crystal structure of kaolinite with respect to unit cell directions 'a' and 'b'. We also carried out calculations using periodic models of a 3-dimensional 1×1×1 crystal and a 2-dimensional 2×2 slab, where all atomic positions and lattice parameters were optimized using the Periodic Boundary Condition (PBC) approach.[33-35] The 2×2 slab model is comparable in number of atoms (144) and electrons (1040) to the presented coordination chemistry-based cluster model (136 and 1040, respectively).

Computational Level of Theories

The density functional theory calculations were carried out using the Gaussian09[36] quantum chemical package. We report here the results obtained by a systematic series of hybrid and pure (GGA) functionals including PW91,[37, 38] which was the level of theory used in the reference structural work.[28] The rational for the selection of HF method,[39] and the B3LYP,[40, 41] BLYP,[40, 42, 43] PW91[37, 38] functionals is illustrated by Scheme 2.

Effective core potentials (ECP: LANL2DZ[44] and SDD[45, 46]) and all electron basis sets (DZ: 6-31G[47, 48] and TZ: def2-TZVP[49, 50]) were used in combinations of polarization and diffuse basis functions. Double-ζ quality basis sets showed the largest structural changes for the position of the *i*-HO^- group and the adjacent Al^{3+} ions. However, their moderate computational costs allowed for the systematic evaluation of structural effects of a wide variety of environmental perturbations, such as neutralizing charges and field of point-charges, and the comparison of the cluster and periodic models. An increase in the completeness of the basis set either by adding polarization[51-53] (ECP* or DZ*) or diffuse[54] functions (DZ+, DZ+*) or considering triple-ζ quality basis sets (TZ) reduced the magnitude of structural changes; however, all trends remained qualitatively the same.

Polarizable continuum model with water-based parameters[55] and explicit water solvent molecules were considered for a brief inquire into solvation effects. Using finer integration grids in DFT calculations and consideration of empirical dispersion correction[56] did not show appreciable effect for the positions of the *i*-HO^- group and adjacent Al^{3+} ions, while these are expected to be important for later studies of surface reactivity.

Constrained Partial Optimizations

The evaluation of differences in the position of the *i*-HO^- group and adjacent Al^{3+} ions and their dependence on the outer

surface environment between the crystalline and exfoliated kaolinite were carried out by partial geometry optimizations. In the background of constrained Cartesian coordinates of the outer sphere atoms, the *i*-HO^- groups were allowed to move followed by a consecutive step of relaxation of the two adjacent Al^{3+} ions. The given cluster model contains four *i*-HO^- groups; however, only one of them is located centrally and has a complete chemical environment (Fig. 1). An outer *i*-HO^- group along the misfit direction between the Al- and Si-honeycombs was also utilized to probe the structural influence of chemical perturbations. Models with a field of point-charges required the conversion of Cartesian to the internal coordinates for the 150-atom model. Optimizations using Z-matrix or Cartesian coordinates resulted identical structures, thus any structural difference between the cage of Na^+/Mg^{2+} ions and a field of point-charges is related to the influence of distant Coulomb interactions of point-charges as defined in Table 1.[57-64]

Results and Discussion

The structural optimizations using ECP and DZ basis sets show a large-scale structural rearrangement for the *i*-HO^- group in the molecular cluster model for the exfoliated OT-sheet regardless of the functional used in comparison to the crystalline kaolinite structure. This can be illustrated by the opening of the O(*s*-HO^-)$\cdots$O-H(*i*-HO^-) angle (α_2) from 120º to more than 158º in the *in vacuo* models, which increases the co-planarity of the *i*-HO^- group with respect to the [$Al^{3+}\cdots$*i*-HO^-/*s*-HO^-]$_2$ rhomb. Upon inspection of the H-bond/charge-dipole interaction network, the main driving force for this distortion is the formation of an ideal H-bonding interaction with a nearly linear O-H(*i*-HO^-)$\cdots$*b*-O^{2-} angle (α_1) and a short 2.56 Å H(*i*-HO^-)$\cdots$*b*-O^{2-} distance (δ) as shown in Table 2. This drastic structural change in the exfoliated kaolinite model relative to the crystalline structure may originate from (i) limitations of the molecular cluster model, (ii) absence of the H-bonding between the adjacent OT-layers, or (iii) the ill-defined nature of Al-OH bonding, since the ECP and DZ basis sets are small and do not contain d-functions to describe the six-coordinate Al^{3+} ions. In the next three sections, we provide a detailed account on how these sources of distortions contribute to the observed changes.

Cluster *versus* Periodic Computational Models

Using the Periodic Boundary Condition approach, we optimized the 1×1×1 unit cell and a 2×2 slab model of crystalline and exfoliated kaolinite, respectively at the PW91/DZ level. The experimental unit cell dimensions of a = 5.154 Å, b = 8.942 Å, c = 7.401 Å; α = 91.7º, β = 104.6º, γ = 89.8º were qualitatively reproduced using a double-ζ quality basis set (5.429 Å, 9.045 Å, 7.393 Å; 92.1º, 97.2º, 92.5º; respectively). However, the 0.3 and 0.1 Å expansion in 'a' and 'b' crystal directions and the deviation of 7º in the angle of unit vectors suggest notable structural distortion within the unit cell. This is manifested by the change in the δ, α_1, and α_2 internal coordinates of the *i*-HO^- group. Addition of polarization function (DZ*) and using a different GGA functional (BP86) or a hybrid GGA functional (B3LYP) results in improved δ distances and α_2 angles; however, this achieved at the expense of the good agreement in α_1 angles.

The deviations between the calculated and the experimental distances (Table 2) become pronounced for the 2×2 periodic slab model, where the interlayer H-bonds are absent as they adapt values that are typically observed for *in vacuo,* i.e. external chemical environment free, cluster model. Inspection of the geometry optimization path of a 1×1×1 periodic crystal model with initial *i*-HO^- group position in ideal H-bond interaction with the *b*-O^{2-} group (minimized δ distance and maximized α angles, Fig. 3A) showed the presence of a local minimum on an energy plateau. This corresponded to an *i*-HO^- position that are observed for the exfoliated kaolinite model. This could be a local minima even in the crystalline structure if the interlayer O-H(*s*-HO^-)$\cdots$*b*-O^{2-} H-bond interactions (Fig. 3B) are incorrectly described. Comparison of the H-bond distances in Fig. 3B shows a large deviation from those of the optimized periodic model structure (Fig. 3C). The structural changes in the periodic and cluster models clearly demonstrate the result of the incomplete modelling or inadequately description of external chemical environment around the surface hydroxide groups and the bridging oxide groups. This directly influences the internal chemical environment of the OT-sheet.

Table 2 Summary of representative internal coordinates from Fig. 1 with respect to the position of the *i*-HO^- group as a function of external chemical environment and levels of theory in the exfoliated OT-sheet of kaolinite

Level of theory	External environment	δ, Å	α_1, º	α_2, º
Experiment[28]	crystalline phase	2.83	127	120
	Periodic models			
PW91/DZ	1×1×1 crystal	3.024	120.8	129.0
BP86/DZ*		3.002	110.3	120.0
B3LYP/DZ*		2.999	111.0	120.7
PW91/DZ*		2.980	110.6	120.8
BP86/DZ	2×2 slab, *in vacuo*	2.497	164.6	146.4
PW91/DZ		2.463	173.9	160.4
	Molecular cluster models			
HF/ECP	*in vacuo*	2.623	163.9	170.0
HF/DZ		2.595	175.1	162.1
B3LYP/ECP		2.558	179.3	158.3
		2.569	175.0	162.3
B3LYP/DZ	PCM(water)	2.688	140.0	158.3
	H_2O fixed[a] at *b*-O^{2-}	2.557	174.9	155.5
	Mg^{2+} fixed[a] at *b*-O^{2-}	2.778	128.8	125.2
	optimized Mg^{2+}	2.830	105.0	102.7
B3LYP/DZ*	*in vacuo*	2.770	132.4	125.2
B3LYP/DZ+,*		2.767	132.7	125.7
B3LYP/ECP*		2.764	132.0	125.3
HF/TZ		2.744	143.8	133.7
B3LYP/TZ		2.727	141.9	132.3
BLYP/TZ		2.698	140.0	130.3
PW91/TZ		2.718	138.3	129.2

[a] *b*-$O^{2-}\cdots OH_2$ or Mg^{2+} ion distance was constrained to 2 Å.

Evaluating the Effect of the External Chemical Environment

In order to map out the limits for how much the external chemical environment can perturb the position of the *i*-HO^- group, we systematically modified the incomplete coordination environment of the *i*-HO^- group outside of the [$Si^{4+}\cdots$*b*-O^{2-}]$_6$ honeycomb-like unit. As shown on the left side of Fig. 1, the possibility of forming an *b*-$O^{2-}\cdots$O-H(*i*-HO^-) interaction does not exist, since the *b*-O^{2-} group from the second outer coordination sphere was not included in the given computational model. This results in a significantly reduced movement of the *i*-HO^- group (less than 10º opening of the α_2 angle) relative to the central *i*-HO^- group with a complete

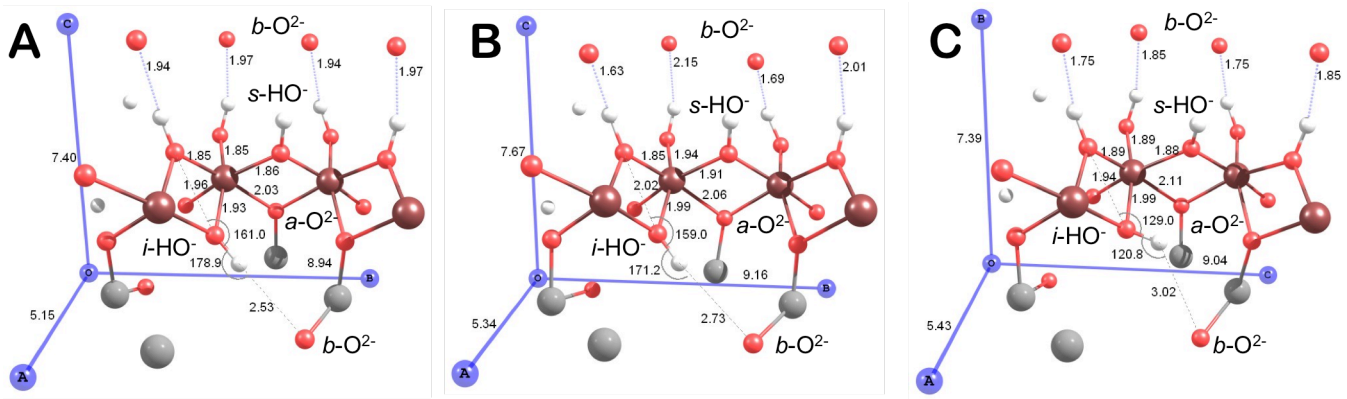

Fig. 3 The 1×1×1 periodic model for crystalline kaolinite with distorted *i*-HO$^-$ position (A), first local minima with distortion maintained by interlayer H-bonding interactions altered (B), and fully optimized structure (C) at PW91/DZ level

chemical environment. Insertion of the missing *b*-O^{2-} group and replacement of the two Mg^{2+} counter ions with Al^{3+} ions for maintaining charge neutrality increases the co-planarity of the *i*-HO$^-$ group ($\Delta\alpha_2$) by 30°. The opposite trend is observed when the two Mg^{2+} counter ions are replaced with Na^+ ions and an additional Mg^{2+} ion was placed at the position of the missing the *b*-O^{2-} group. The electrostatic repulsion between positive counter ions and the positive end of the *i*-HO$^-$ bond dipole results in a more perpendicular arrangement of the O-H(*i*-HO$^-$) bond and the [Al^{3+}···*i*-HO$^-$/*s*-HO$^-$]$_2$ rhomb as indicated by the decrease of the α_2 angle by 3° relative to the crystallographic value of 120°. The changes of *i*-HO$^-$ group's positions and involvement in H-bonding or charge/dipole interactions can be probed by band positions and intensities from IR spectroscopy[65]

An experimentally relevant structural perturbation is the modification of the outer chemical environment around the *b*-O^{2-} group (Fig. 1) that is adjacent to the *i*-HO$^-$ group of interest. In the crystalline phase, strong H-bonding interactions keep the OT layers together at about 2.9-3.0 Å O(*s*-HO$^-$)···*b*-O^{2-} distances. These reduce the nucleophilicity of the *b*-O^{2-} group at the advantage of inner *a*-O^{2-} groups than can engage in charge/dipole interactions with the *i*-HO$^-$ group. The presence of four *a*-O^{2-} groups (Fig. 2B) results in the co-parallel arrangement of the H-O bond of the *i*-HO$^-$ group with the plane of the OT-sheet. Embedding the computational model into a water solvent-based polarizable continuum model shrouds all *b*-O^{2-} groups with a field of electrostatic interactions, and thus the movement of the *i*-HO$^-$ group is approximately halved relative to the *in vacuo* model. Addition of an explicit solvent water molecule at fixed *b*-O^{2-}···HOH distance of 2 Å resulted in similar changes to the *in vacuo* model by opening the O(*s*-HO$^-$)···O-H(*i*-HO$^-$) angle α_2 to 155° and forming an ideal linear H-bond between the *b*-O^{2-} and *i*-HO$^-$ with α_1 = 175°. Given the strong influence of electrostatic interactions, we have evaluated the effect of the presence of a cation adjacent to the *b*-O^{2-} group by including an additional Mg^{2+} ion into the model. When its position was fixed at 2 Å distance from the *b*-O^{2-} group, the movement of the *i*-HO$^-$ group was practically eliminated. The collective covalent and ionic effects of the interlayer H-bonding network in the crystalline kaolinite can be compared to the ionic effect of a divalent cation at 2 Å. Upon release of the Mg^{2+}···*b*-O^{2-} constraint, the Mg^{2+} ion migrates toward the middle of the Si-honeycomb, enters inside the T-sheet, and pulls on the O atom of the *i*-HO$^-$ group to form a Mg^{2+}···O(*i*-HO$^-$) distance of 2.28 Å. This results in an opposite effect for the H-O(*i*-HO$^-$)···O(*s*-HO$^-$) α_2 angle than those observed above, since this angle is now reduced by 18° relative to that in the crystal structure. The magnitude of the change is likely exaggerated due to the limitation of the ECP and DZ basis set (see below). Such structural changes lend support to a hypothesis that the outer surface or interlayer interactions can considerably affect the chemical environment of the buried *i*-HO$^-$ group and thus its structural properties. Furthermore, the spontaneous migration of cation inside the OT-sheet is also an experimentally relevant observation with regards of intercalation of carboxylate salts.[1]

Sensitivity of Inner Hydroxide Positions to Level of Theory

The lack of d-orbitals in the ECP and DZ basis sets biases the relative importance of ionic charge/charge, charge/dipole, dipole/dipole, and H-bonding interactions *versus* covalent Al-O bonding that are non-negligible for the hexacoordinate Al^{3+} ions, and μ_3-coordinate oxide anions. This can be remedied by the inclusion of polarization functions in the form of additional d-function to O, Al, and Si. As expected, the extension of the basis set reduced the structural changes in comparison to the DZ/ECP results. The calculated internal coordinates in the exfoliated OT-layer were within 0.06 Å and 5° of the crystalline structure. Polarization functions for H atoms and diffuse functions for all atoms do not affect the position of the *i*-HO$^-$ groups to an appreciable degree relative to the results of single set of polarization functions on heavy atoms.

As the highest level of theory of the given study, we carried out calculations with all-electron triple-ζ basis set (TZ) with polarization function for all atoms. It is remarkable to notice that the optimized values (Table 2) for the monitored distances (δ) and angles (α_1, α_2) (Fig. 1) fall between those obtained for the DZ/ECP basis sets with and without polarization functions. This indicate that neither the DZ/ECP nor the DZ*/ECP* basis sets can be considered as saturated with respect to the positions of the *i*-HO$^-$ and the two adjacent Al^{3+} ions. At the B3LYP/TZ level, δ distance is about 0.1 Å shorter and the α_1, α_2 angles open up by only 12-14° in the exfoliated OT-layer of kaolinite relative to the crystal structure. Considering the trend in molecular geometry as a function of DZ/ECP, DZ*/ECP*, and TZ basis sets, the results suggest an experimentally measurable response in the *i*-HO$^-$ group positions as a function of the external chemical environment. This has already been indicated by IR spectroscopic data that indicate small, but significant differences between the inner hydroxide stretching frequencies

Table 3 Summary of representative internal coordinates from Fig. 1 with respect to the position of the *i*-HO^- group as a function of neutralizing charges calculated at the HF/DZ level of theory in the exfoliated OT-sheet of kaolinite (internal coordinates: d = 2.83 Å, α_1 = 127º, α_2 = 120º in the crystalline phase)

Neutralizing counter ions	δ, Å	α_1, º	α_2, º
Li^+/Be^{2+} counter ions	2.601	171.6	164.6
Na^+/Mg^{2+} counter ions	2.595	175.1	162.1
K^+/Ca^{2+} counter ions	2.623	163.9	170.0
Cs^+/Ba^{2+} counter ions	2.646	159.2	172.8
no counter ions (Cartesian)	2.743	136.9	132.1
no counter ions (Z-matrix)	2.719	140.2	134.3
PCM w/o counter ions	2.706	140.7	131.3
PCM w/Na^+/Mg^{2+} ions	2.703	142.7	132.8
+1 and +2 point-charges	2.598	175.4	161.8
point-charges form ionic limit	2.721	174.2	142.7
QEq point-charges	2.583	177.8	159.4
PM6 point-charges	2.592	164.5	171.4
PW91/MPA point-charges	2.575	172.9	156.2
PW91/NPA point-charges	2.656	151.9	178.8

in kaolinite (3620 cm^{-1}), dickite (3622 cm^{-1}), and nacrite (3629 cm^{-1}) with different interlayer chemical environments.[66] Furthermore, these results emphasize the need of using at least triple-ζ quality basis sets for describing the structural properties of clay cluster models, since smaller basis sets even with polarization and diffuse functions give considerable different structures for the exfoliated kaolinite.

Keeping in mind the delicate balance between the ionic and covalent components of chemical bonds in kaolinite, we also evaluated the dependence of the structural parameters on the composition of the density functionals. As described in the Methods Section, the reference level is the ionic HF wave function method. This was then extended toward a more covalent B3LYP hybrid functional, and then the most covalent BLYP and PW91 functionals among the considered ones. From the middle section of Table 2, it is remarkable to notice that the position of the *i*-HO^- group changes rather similarly regardless of the functional within 0.04 Å and 6º. The most ionic HF calculations give the longest δ distance, the largest α_1 and α_2 angles. As the amount of density functional exchange component increases at the expense of the HF exchange in the hybrid functional, the *i*-HO^- group moves slightly closer to the *b*-O^{2-} group. This can be explained by the effect of the increasing importance of covalent interactions that maximize the overlap by reducing interatomic distances. However, this cannot be maximized, since the Al^{3+}-O(*i*-HO^-) covalent interactions will moderate the angular changes as manifested by the decrease of the α angles in going from HF to BLYP method. We found negligible differences among the different GGA functionals (BLYP and PW91) within 0.02 Å and 2º with respect to δ and α internal coordinates.

Counter Ion Effects

The importance of balancing the covalent and ionic interactions can also be assessed by the effect of charge neutralizing cations at the periphery of the model. Calculations presented in Table 2 were carried out using Na^+ and Mg^{2+} ions at the position of Al^{3+} and Si^{4+} ions, respectively, from the third coordination sphere environment of the central O-sheet honeycomb. These counter ions present a compromise in ionic radius and radial wave functions for n = 3 with respect to the native cations. The use of smaller (Li^+/Be^{2+}) and gradually larger (K^+/Ca^{2+} and then Cs^+/Ba^{2+}) ions with mismatch in the principal quantum numbers of the valence orbitals relative to the Al^{3+}/Si^{4+} pair displays a non-linear trend in Table 3, since both the smaller and larger cations give longer δ distances, smaller α_1 and larger α_2 values. The overall range for explicit counter ion effect is $\Delta\delta \approx 0.05$ Å and $\Delta\alpha \approx 8$º. When no counter ions are used, the computational model is flooded with a -28 negative charge, which reduces the polarity of the H-O bond, and thus its affinity to engage in H-bonding interactions. Therefore, only moderate structural distortions are observed of $\Delta\delta \approx 0.1$ Å and $\Delta\alpha \approx 10$º relative to the model with Na^+/Mg^{2+} ions. Upon addition of a polarizable continuum model with high dielectric environment (water) to the highly anionic model, the *a*-$O^{2-}\cdots$H-O(*i*-HO^-) distance δ further contracts by 0.03 Å and the corresponding angle α_1 opens by 4º. It is notable that addition of Na^+/Mg^{2+} counter ions at the periphery of the model does not significantly affect the position of the *i*-HO^- group. This can be rationalized by the overwhelming effect of the electrostatic interactions with the polarizable continuum at shorter distances above and below the OT-sheet, compared with the polarizing effect of the Na^+/Mg^{2+} counter ions through inner and outer coordination spheres.

In order to evaluate whether the neutralizing cage of point-charges is a reasonable model for capturing the electrostatic effects for the inner hydroxide moiety at 5-7 Å from the periphery, we have carried out further structural optimization using a sizeable field of point-charges obtained by various methods (Table 1) representing different degrees of charge separation. Generally, the most polarized charge distribution according to the formal point-charges for example, trigger the largest structural distortions in the exfoliated kaolinite, while the less polarized field provides results comparable to those without any counter ions present. Overall, all point-charge calculation indicated the deviation in the *i*-HO^- position in the exfoliated OT-sheet compared to the crystalline kaolinite structure. Thus, the given systematic benchmarking study for the effect of counter ions justifies the use of Na^+ and Mg^{2+} ions as a chemically reasonable cage of neutralizing charges.

Counterintuitive Al-O Distances in Crystalline Kaolinite

Fig. 4 summarizes the average displacements of atoms in the optimized cluster models for the exfoliated kaolinite relative to their positions determined by X-ray and neutron diffraction for the crystalline kaolinite.[28] The displacements of 0.09 Å, 0.04 Å, and 0.38 Å for the two Al^{3+} ions, O and H atoms of the *i*-HO^- group, respectively, correspond to shortening of the *b*-$O^{2-}\cdots$H-O(*i*-HO^-) distance (δ) by 0.27 Å, 48º and 40° opening of the *b*-$O^{2-}\cdots$H-O(*i*-HO^-) and H-O(*i*-HO^-)$\cdots$O(*s*-HO^-) angle (α_1 and α_2), respectively at the B3LYP/DZ level. While there are variations in the positions for the H and O atoms as a function of external chemical environment and level of theory, the Al^{3+} ion displacements in the exfoliated relative to the crystalline kaolinite are practically independent from the computational model and method. The absolute displacement of about 0.1 Å for the Al^{3+} ions is quite significant. This corresponds to the sinking of Al^{3+} ions along the 'c' crystal axis, which is approximately the normal of the (001) plane of the crystalline kaolinite independently from the magnitude of the *i*-HO^- rearrangement.

Table 4 Summary of experimental and calculated Al-O distances (Å) for the crystalline and exfoliated OT-layer of kaolinite, respectively

		O(s-HO$^-$)			average	O(i-HO$^-$)	a-O^{2-}		average
	levels of theory	vicinal	geminal	distal	s-HO$^-$		proximal	distal	a-O^{2-}
crystalline	experimental	1.86	1.85	1.85	1.86	1.93	2.03	1.96	1.98
				Periodic models					
	PW91/DZ	1.891	1.876	1.894	1.887	1.993	2.113	1.948	2.031
crystalline	BP86/DZ*	1.878	1.884	1.899	1.887	1.971	2.075	1.939	2.007
1×1×1	B3LYP/DZ*	1.866	1.879	1.895	1.880	1.962	2.077	1.916	1.996
	PW91/DZ*	1.877	1.885	1.896	1.886	1.965	2.074	1.937	2.005
exfoliated	BP86/DZ	1.895	1.942	1.928	1.922	1.909	1.955	1.943	1.949
2×2	PW91/DZ	1.940	1.922	1.939	1.934	1.935	1.961	1.968	1.965
				Cluster models					
	B3LYP/DZ	1.928	1.916	1.893	1.912	1.893	1.969	1.884	1.915
	B3LYP/DZ*	1.933	1.916	1.890	1.913	1.890	1.970	1.878	1.913
	B3LYP/DZ+,*	1.931	1.917	1.891	1.913	1.888	1.968	1.881	1.912
exfoliated	HF/TZ	1.938	1.916	1.880	1.911	1.869	1.972	1.880	1.907
	B3LYP/TZ	1.930	1.914	1.886	1.910	1.880	1.971	1.881	1.911
	BLYP/TZ	1.923	1.915	1.889	1.909	1.897	1.969	1.889	1.918
	PW91/TZ	1.926	1.914	1.890	1.910	1.890	1.971	1.886	1.916

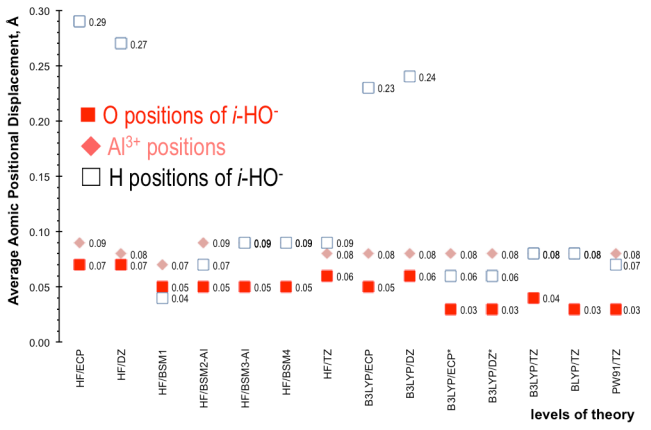

Fig. 4 Graphical summary of average atomic positional displacements for i-HO$^-$ groups and adjacent Al^{3+} ions

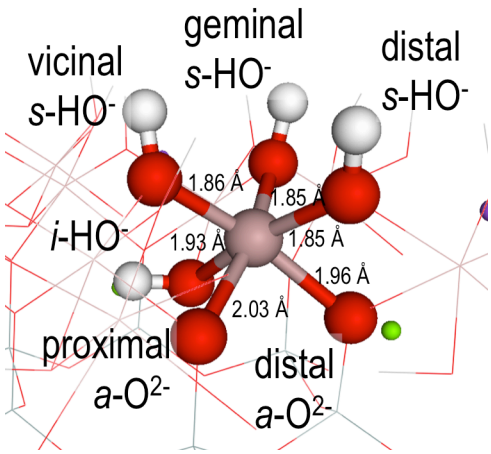

Fig. 5 Inner coordination sphere of the Al^{3+} ions

A closer inspection of the experimental Al-O distances for the inner coordination sphere of the Al^{3+} ion (Fig. 5) reveals counterintuitive trends. From metal/group (M/L) charge differences, the O^{2-}···Al^{3+} bond is expected to be shorter than the HO$^-$···Al^{3+} even with the consideration of the μ^3- and μ^2-bridged natures of the oxide and hydroxide groups, respectively. The shorter (1.85-1.86 Å) Al-O distances correspond to the three Al^{3+}···O(s-HO$^-$) bonds. A group of considerably longer distances toward the T-sheet is formed by Al^{3+}···O(i-HO$^-$) of 1.93 Å, the Al^{3+}···a-O^{2-} distances of 1.96-2.03 Å. Table 4 summarizes the numerical changes in the coordination environment of the Al^{3+} ions as a function of levels of theory and computational models, when the i-HO$^-$ groups and the two adjacent Al^{3+} ions were allowed to move, while everything else were kept at their crystallographic positions. We can see a considerable difference between the outer and inner Al-O distances from comparison of the initial, the partially optimized, and fully optimized periodic structures of the crystalline kaolinite in Fig. 3 as a function of the treatment and modelling of H-bonding interactions between adjacent OT-layers. In contrast, the optimization of the periodic 2×2 slab model resulted a similar reduction between the Al-O distances as in the molecular cluster model (Table 4) regardless of the specific level of theory.

Calculations for the cluster model of the exfoliated kaolinite show about 0.03-0.07 Å elongation of the Al^{3+}···O(s-HO$^-$) distances, while shortening of the Al^{3+}···O(i-HO$^-$) and Al^{3+}···a-O^{2-} distances by 0.05-0.08 Å independently from the density functional and the basis set used. The average value of the experimentally observed differences in the surface and inner Al-O distances of 0.12 Å (Fig. 5) is eliminated (less then 0.01 Å) after optimization (Table 4, average values).

Since the equalisation of the Al-O bond lengths was observed at all levels of theory for the exfoliated kaolinite models and asymmetry in the Al-O bonds for the periodic crystal model, we propose that the counterintuitive Al-O distances are associated with the presence of strong interactions from the external chemical environment. These result in the

shortening of the surface Al-O and lengthening of the inner and apical Al-O distances. With respect to morphology, this can be illustrated by pliability of the OT-layer in exfoliated kaolinite as a function of external chemical environment. The interconnectedness of the chemical interactions within and in between OT-layers can be described as follows: i) in crystalline phase with strong H-bonding between OT layers, the H-bond acceptor *b*-O^{2-} group of an adjacent T-sheet shares its electron density with the interacting H atom of the *s*-HO^- group, ii) the $Al^{3+}\cdots O(s\text{-}HO^-)$ distances become short due to the electron richness of the *s*-HO^- group, iii) the Si^{4+} ions of the adjacent T-sheet compensate the loss of electron density by enhancing the bonding interaction with the *a*-O^{2-} groups, iv) this weakens the Al-O bonds with the μ^3 coordinated *a*-O^{2-} group; and iv) resulting in elongated inner $Al^{3+}\ldots a\text{-}O^{2-}$ distances relative to the outer $Al^{3+}\cdots O(s\text{-}HO^-)$. In the computational model of the exfoliated kaolinite without the presence of strong external chemical environmental effects, the up to 0.08 Å differences for the inter-layer Al-O bond lengths do not take place. This results in the Al^{3+} ions adapting a coordination environment with more balanced Al-O distances and more compact, thus less pliable morphologically. However, when the exfoliated kaolinite layer is embedded in an external environment with strong H-bonding/dipole/charge interactions it will regain its pliability and likely extends through multiple layers.

Conclusions

We have carried out a systematic model building for a molecular cluster model with 156 atoms focused on the honeycomb-like unit of $[Al^{3+}\cdots s\text{-}HO^-]_6$, which is the preferred adsorption site at the O-sheet for many reagents in intercalation and delamination processes. The construction of the model was guided by general coordination chemical principles *versus* availability of computational resources. We presented the case for the need of considering atoms up to the second coordination sphere relative to the central honeycomb-like unit. This model can be terminated by Na^+ and Mg^{2+} counter ions at the position of Al^{3+} and Si^{4+} ions from the third coordination sphere to achieve charge neutrality. The molecular cluster model described here is comparable in size with periodic slab models with 2×2 unit cell dimensions for kaolinite.

The position and orientation of inner hydroxide group and its adjacent Al^{3+} ions provide an opportunity for studying the effects of external chemical environment and the level of theory dependence. In the current model, these have compositionally complete coordination environments with respect to the kaolinite structure. This is not an arbitrary choice since changes in the chemical environment of inner hydroxide groups can be followed by vibrational spectroscopy. We observed experimentally detectable changes in the orientation of the *i*-HO^- group depending on the presence of various ions and molecules at the outer surface of the T-sheet. Furthermore, we document a remarkably strong basis set effect with at least a triple-ζ quality basis being reasonable for describing the structural features of the central moiety. On the contrary, HF, hybrid, and 'pure' DFT calculations using the same basis set resulted in practically identical optimized structures. Evaluation of the effect of the neutralizing counter ion compositions revealed that the substitution of Al^{3+}/Si^{4+} ions in the third coordination sphere from the moiety of interest with Na^+/Mg^{2+} ions is a reasonable compromise with respect to ionic radius and covalent orbital interactions. These were confirmed by results obtained by using a field of 460 point-charges.

All *in vacuo* calculations showed sinking of the Al^{3+} ions toward the centre of the OT-layer in the exfoliated kaolinite model regardless of the employed basis set or the functional giving balanced surface and inner Al-O distances. Analysis of the differences in bond lengths in the experimental structure, calculated periodic crystalline, and molecular cluster structure revealed a chain of interconnected bonds (surface HO-Al, Al-apical O, apical O-Si) that can transmit effects from external chemical environment toward the inner layers.

The above computational results allowed us to propose two experimentally testable hypotheses, which are the subjects of our on going vibrational spectroscopic, X-ray absorption spectroscopic, and thermal analytical investigations on exfoliated kaolinite samples. The sensitivity of the position and orientation of the inner hydroxide group suggests a spectator role for the external chemical environment due to its network of interactions with the apical and bridging oxide ligands and the two adjacent Al^{3+} ions. Furthermore, strong interactions with the surface hydroxide groups can be transmitted through the OT-layer *via* a cascade of alternating degrees of bond altering events. This can result in the movement of Al^{3+} ions of the O-sheet, thus changes in electronic structure of bridging oxides of the T-sheet, and perturbation of surface hydroxides from the adjacent OT-layer. This provides a plausible mechanistic step for weakening the inner-layer hydrogen bonding interactions when a strongly interacting external chemical environment is present, and thus preparing the OT-layers of crystalline kaolinite for opening up for intercalation.

Acknowledgements

This research was supported by the European Union and the State of Hungary, co-financed by the European Social Fund in the framework of TÁMOP-4.2.2.A-11/1/KONV-2012-0071 (AT and RK) and TÁMOP 4.2.4.A/2-11-1-2012-0001 'National Excellence Program' (RKS). The authors acknowledge the helpful discussions with Prof. János Kristóf and Prof. Erzsébet Horváth. We acknowledge the use of the computational facilities at Montana State University, Bozeman, MT and National Information Infrastructure Development (NIIF) Program of Hungary.

Notes and references

[a] Department of Environmental Engineering, Faculty of Engineering, University of Pannonia, Veszprém, H-8201, PO Box 10, Hungary
[b] Department of Analytical Chemistry, Faculty of Engineering, University of Pannonia, Veszprém, H-8201, PO Box 10. Hungary, Fax: +36 88 624-194, E-mail: szilagyi@almos.uni-pannon.hu, Homepage: http://sci-res.blog.hu/
[c] Department of Chemistry and Biochemistry, Montana State University, Bozeman, MT 59718, U.S.A.

Electronic Supplementary Information (ESI) available: Cartesian coordinates of the coordination chemical models, formatted checkpoint files are available from http://computational.chemistry.montana.edu/SI.

1 R. Frost and J. Kristóf, in *Interface Science and Technology* eds. F. Wypych and K. G. Satyanarayana, Elsevier-Academic Press, 2004, vol. Vol 1 (Clay Surfaces – Fundamentals and Applications), pp. 184-215.
2 L. Benco, D. Tunega, J. Hafner and H. Lischka, *American Mineral.*, 2001, **86**, 1057-1065.
3 L. Benco, D. Tunega, J. Hafner and H. Lischka, *J. Phys. Chem. B*, 2001, **105**, 10812-10817.

4 H. Sato, K. Ono, C. T. Johnston and A. Yamagishi, *American Mineral.*, 2005, **90**, 1824-1826.
5 A. Michalkova and D. Tunega, *J. Phys. Chem. C*, 2007, **111**, 11259-11266.
6 B. Civalleri, P. Ugliengo, C. M. Zicovich-Wilson and R. Dovesi, *Z. Kristallog.*, 2009, **224**, 241-250.
7 P. Ugliengo, C. M. Zicovich-Wilson, S. Tosoni and B. Civalleri, *J. Mat. Chem.*, 2009, **19**, 2564-2572.
8 C. E. White, J. L. Provis, D. P. Riley, G. J. Kearley and J. S. J. van Deventer, *J. Phys. Chem. B*, 2009, **113**, 6756-6765.
9 L. Smrcok, D. Tunega, A. J. Ramirez-Cuesta, A. Ivanov and J. Valuchova, *Clays Clay Mineral.,* 2010, **58**, 52-61.
10 P. H. J. Mercier and Y. Le Page, *Eur. J. Mineral.*, 2011, **23**, 401-407.
11 D. L. Geatches, A. Jacquet, S. J. Clark and H. C. Greenwell, *J. Phys. Chem. C*, 2012, **116**, 22365-22374.
12 D. Tunega, T. Bucko and A. Zaoui, *J. Chem. Phys.*, 2012, **137**.
13 Z. Hato, E. Mako and T. Kristof, *J. Mol. Mod.*, 2014, **20**, 10.
14 A. Pelmenschikov and J. Leszczynski, *J. Phys. Chem. B*, 1999, **103**, 6886-6890.
15 E. A. S. Castro and J. B. L. Martins, *Int. J. Quant. Chem.*, 2005, **103**, 550-556.
16 R. B. Campos, F. Wypych and H. P. Martins, *Int. J. Quant. Chem.*, 2009, **109**, 594-604.
17 A. Michalkova, T. L. Robinson and J. Leszczynski, *Phys. Chem. Chem. Phys.*, 2011, **13**, 7862-7881.
18 M. M. Dawley, A. M. Scott, F. C. Hill, J. Leszczynski and T. M. Orlando, *J. Phys. Chem. C*, 2012, **116**, 23981-23991.
19 A. M. Scott, M. M. Dawley, T. M. Orlando, F. C. Hill and J. Leszczynski, *J. Phys. Chem. C*, 2012, **116**, 23992-24005.
20 Y. R. Jiang and X. X. Li, *Sep. Purif. Technol.*, 2013, **104**, 114-120.
21 K. H. Song, X. Wang, P. Qian, C. Zhang and Q. Zhang, *Comp. Theor. Chem.*, 2013, **1020**, 72-80.
22 X. Wang and P. Qian, *Chem J. Chinese Uni.-Chinese*, 2013, **34**, 2601-2608.
23 Y. Park, G. A. Ayoko, R. Kurdi, E. Horvath, J. Kristof and R. L. Frost, *J. Colloid Interface Sci.*, 2013, **406**, 196-208.
24 E. Mako, J. Kristof, E. Horvath and V. Vagvolgyi, *Appl. Clay Sci.*, 2013, **83-84**, 24-31.
25 T. V. Harris and R. K. Szilagyi, *Inorg. Chem.*, 2011, **50**, 4811-4824.
26 A. S. Pandey, T. V. Harris, L. J. Giles, J. W. Peters and R. K. Szilagyi, *J. Am. Chem. Soc.*, 2008, **130**, 4533-4540.
27 D. Rokhsana, D. M. Dooley and R. K. Szilagyi, *J. Biol. Inorg. Chem.*, 2008, **13**, 371-383.
28 L. Smrcok, D. Tunega, A. J. Ramirez-Cuesta and E. Scholtzova, *Phys. Chem. Minerals*, 2010, **37**, 571-579.
29 A. Belsky, M. Hellenbrandt, V. L. Karen and P. Luksch, *Acta Crystallog. Section B - Struct. Sci.*, 2002, **58**, 364-369.
30 G. Bergerhoff, R. Hundt, R. Sievers and I. D. Brown, *J. Chem. Inf. Comput. Sci.*, 1983, **23**, 66-69.
31 X. Wang, P. Qian, K. H. Song, C. Zhang and J. Dong, *Comp. Theor. Chem.*, 2013, **1025**, 16-23.
32 J. Tokarsky, P. Capkova and J. V. Burda, *J. Mol. Mod.*, 2012, **18**, 2689-2698.
33 K. N. Kudin and G. E. Scuseria, *Chem. Phys. Lett.*, 1998, **289**, 611-616.
34 K. N. Kudin and G. E. Scuseria, *Phys. Rev. B*, 2000, **61**, 16440-16453.
35 K. N. Kudin, G. E. Scuseria and H. B. Schlegel, *J. Chem. Phys.*, 2001, **114**, 2919-2923.
36 M. J. T. Frisch, G. W.; Schlegel, H. B.; Scuseria, G. E.; Robb, M. A.; Cheeseman, J. R.; Scalmani, G.; Barone, V.; Mennucci, B.; Petersson, G. A.; *et alas Gaussian 09*, (2009) Gaussian, Inc., Wallingford CT.
37 J. P. Perdew and Y. Wang, *Phys. Rev. B*, 1992, **45**, 13244-13249.
38 J. P. Perdew, J. A. Chevary, S. H. Vosko, K. A. Jackson, M. R. Pederson, D. J. Singh and C. Fiolhais, *Phys. Rev. B*, 1992, **46**, 6671-6687.
39 J. C. Slater, *Phys. Rev.*, 1951, **81**, 385-390.
40 C. T. Lee, W. T. Yang and R. G. Parr, *Phys. Rev. B*, 1988, **37**, 785-789.
41 A. D. Becke, *J. Chem. Phys.*, 1993, **98**, 5648-5652.
42 B. Miehlich, A. Savin, H. Stoll and H. Preuss, *Chem. Phys. Lett.*, 1989, **157**, 200-206.
43 A. D. Becke, *Phys. Rev. A*, 1988, **38**, 3098-3100.
44 T. H. Dunning Jr. and P. J. Hay, ed. H. F. Schaefer III, Plenum, New York 1976, vol. 3, pp. 1-28.
45 P. Fuentealba, H. Stoll, L. von Szentpaly, P. Schwerdtfeger and H. Preuss, *J. Phys. B - At. Mol. Opt. Phys.*, 1983, **16**, L323-L328.
46 P. Fuentealba, H. Preuss, H. Stoll and L. von Szentpaly, *Chem. Phys. Lett.*, 1982, **89**, 418-422.
47 R. Ditchfield, W. J. Hehre and J. A. Pople, *J. Chem. Phys.*, 1971, **54**, 724-728.
48 W. J. Hehre, R. Ditchfield and J. A. Pople, *J. Chem. Phys.*, 1972, **56**, 2257-2261.
49 A. Schäfer, H. Horn and R. Ahlrichs, *J. Chem. Phys.*, 1992, **97**, 2571-2577.
50 A. Schäfer, C. Huber and R. Ahlrichs, *J. Chem. Phys.*, 1994, **100**, 5829-5835.
51 K. L. Schuchardt, B. T. Didier, T. Elsethagen, L. S. Sun, V. Gurumoorthi, J. Chase, J. Li and T. L. Windus, *J. Chem Inf. Model.*, 2007, **47**, 1045-1052.
52 A. Hollwarth, M. Bohme, S. Dapprich, A. W. Ehlers, A. Gobbi, V. Jonas, K. F. Kohler, R. Stegmann, A. Veldkamp and G. Frenking, *Chem. Phys. Lett.*, 1994, **224**, 603-603.
53 A. Hollwarth, M. Bohme, S. Dapprich, A. W. Ehlers, A. Gobbi, V. Jonas, K. F. Kohler, R. Stegmann, A. Veldkamp and G. Frenking, *Chem. Phys. Lett.*, 1993, **208**, 237-240.
54 T. Clark, J. Chandrasekhar, G. W. Spitznagel and P. V. Schleyer, *J. Comp. Chem.*, 1983, **4**, 294-301.
55 J. Tomasi, R. Cammi, B. Mennucci, C. Cappelli and S. Corni, *Phys. Chem. Chem. Phys.*, 2002, **4**, 5697-5712.
56 S. Grimme, *J. Comp. Chem.*, 2006, **27**, 1787-1799.
57 A. K. Rappe, C. J. Casewit, K. S. Colwell, W. A. Goddard and W. M. Skiff, *J. Am. Chem. Soc.*, 1992, **114**, 10024-10035.
58 A. K. Rappe and W. A. Goddard, *J. Phys. Chem.*, 1991, **95**, 3358-3363.
59 J. J. P. Stewart, *J. Mol. Mod.*, 2007, **13**, 1173-1213.
60 J. J. P. Stewart, *J. Mol. Mod.*, 2008, **14**, 499-535.
61 R. S. Mulliken, *J. Chem. Phys.*, 1955, **23**, 1833-1840.
62 J. E. Carpenter and F. Weinhold, *J. Am. Chem. Soc.*, 1988, **110**, 368-372.
63 J. P. Foster and F. Weinhold, *J. Am. Chem. Soc.*, 1980, **102**, 7211-7218.
64 A. E. Reed, L. A. Curtiss and F. Weinhold, *Chem. Rev.*, 1988, **88**, 899-926.
65 E. Horvath, J. Kristof and R. L. Frost, *Appl. Spectrosc. Rev.*, 2010, **45**, 130-147.
66 V. C. Farmer, *The Infrared Spectra of Minerals*, Mineralogical Society, London, 1974.

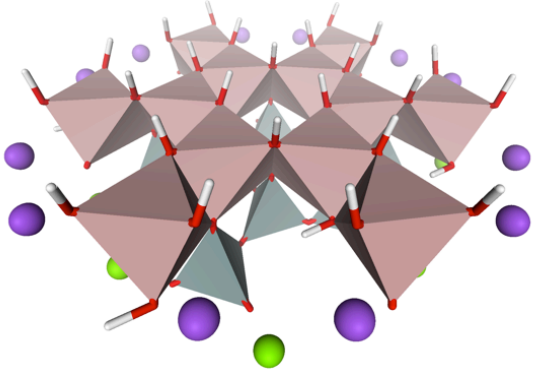

Coordination Chemical Model of Exfoliated Kaolinite

$Na_{12}Mg_8Al_{12}Si_8H_{32}O_{64}$ ~ 2 nm diameter

Pink octahedron: Al(III) sites

Gray tetrahedron: Si(IV) sites

Red: apical and bridging oxide groups

Red and white: surface and inner hydroxide groups

Purple and green spheres are neutralizing K^+ and Mg^{2+} counter ions